#### Research Article

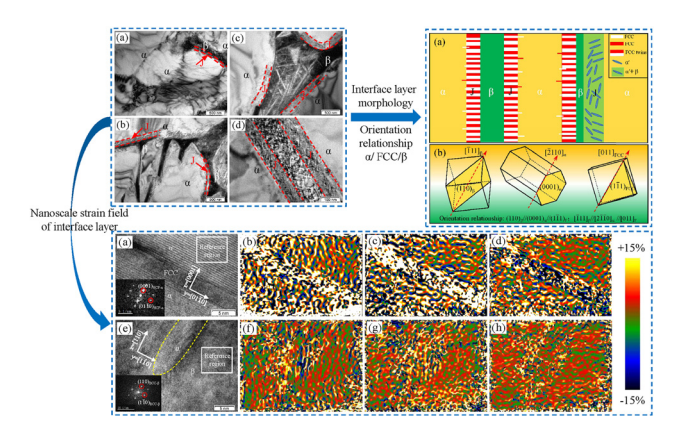
Longlong Lu, Yanmin Zhang\*, Kexing Song\*, Xiuhua Guo, Yan Li, Shangguang Li, and Fei Zhou

# Structural characterization and nanoscale strain field analysis of $\alpha/\beta$ interface layer of a near $\alpha$ titanium alloy

https://doi.org/10.1515/ntrev-2021-0085 received July 17, 2021; accepted September 10, 2021

Abstract: In this article, the structural and nanoscale strain field of the  $\alpha/\beta$  phase interface layer in Ti80 alloy were studied by using high-resolution transmission electron microscopy (HRTEM) and geometric phase analysis (GPA). The  $\alpha/\beta$  interface layer was observed in forged and different annealed Ti80 alloys, which is mainly composed of lamellar face-centered cubic (FCC) phase region and  $\alpha' + \beta$  region. The FCC phases between  $\alpha$  and  $\beta$  phases show a twin relationship, and the twinning plane is  $(1\bar{1}1)$ . The orientation relationship of the  $\beta$  phase, the  $\alpha$  phase, and the FCC phase is  $(110)_{\rm B}//(0001)_{\rm \alpha}//(1\bar{1}1)_{\rm FCC}$  and  $[\bar{1}11]_{\rm B}//$  $[2\bar{1}\bar{1}0]_{\alpha}//[011]_{FCC}$ . The nanoscale strain field of FCC +  $\alpha$ and  $\beta + \alpha'$  regions was analyzed by using the GPA technology. The FCC +  $\alpha$  region shows more significant strain gradient than the  $\alpha' + \beta$  region, and  $\varepsilon_{FCC} > \varepsilon_{\alpha}$ ,  $\varepsilon_{\alpha'} > \varepsilon_{\beta}$ . The influence of element addition on the formation mechanism

Longlong Lu, Xiuhua Guo, Yan Li, Shangguang Li, Fei Zhou: School of Materials Science and Engineering, Henan University of Science and Technology, Luoyang 471023, China; Provincial and Ministerial Co-construction Collaborative Innovation Center of Nonferrous New Materials and Advanced Processing Technology, Luoyang 471023, China; Henan Province Key Laboratory of Nonferrous Materials Science and Processing Technology, Luoyang 471023, China



**Graphical abstract** 

of the FCC phase was discussed. The addition of Zr promotes the formation of the FCC phase by inducing lattice distortion and reducing the stacking fault energy of the  $\alpha$  phase. In addition, the Al element forms an obvious concentration gradient around the interface layer during the cooling process of the alloy, which provides a driving force for the formation of the FCC phase.

Keywords: Ti80 alloy, interface layer, HRTEM, FCC phase, GPA

### 1 Introduction

Titanium and titanium alloys are widely used in aerospace, biomedicine, shipbuilding, and other fields due to their high specific strength, excellent corrosion resistance, and high-temperature mechanical properties [1–4]. The mechanical properties of titanium alloys are mainly controlled by phase composition [5,6], such as the  $\alpha$  phase with hexagonal close-packed (HCP) structure, the  $\beta$  phase with body-centered cubic (BCC) structure, non-close-packed hexagonal  $\omega$  phase, and so on. Recently, the  $\alpha/\beta$  interface layers were observed in pure titanium and titanium alloys [7], which mainly composed of the face-centered cubic (FCC) phase [8]. However, currently, there is no systematic study on the interface layer and the FCC phase of near  $\alpha$  titanium alloy.

<sup>\*</sup> Corresponding author: Yanmin Zhang, School of Materials Science and Engineering, Henan University of Science and Technology, Luoyang 471023, China; Provincial and Ministerial Coconstruction Collaborative Innovation Center of Nonferrous New Materials and Advanced Processing Technology, Luoyang 471023, China; Henan Province Key Laboratory of Nonferrous Materials Science and Processing Technology, Luoyang 471023, China, e-mail: zhangmin70@163.com

<sup>\*</sup> Corresponding author: Kexing Song, School of Materials Science and Engineering, Henan University of Science and Technology, Luoyang 471023, China; Provincial and Ministerial Co-construction Collaborative Innovation Center of Nonferrous New Materials and Advanced Processing Technology, Luoyang 471023, China; Henan Province Key Laboratory of Nonferrous Materials Science and Processing Technology, Luoyang 471023, China, e-mail: kxsong@haust.edu.cn

Early scholars proposed that the interface layer and the FCC phase may be an artificial product formed during the preparation of thin foils examined for transmission electron microscopy [9,10]. However, soon after, Aguayo et al. [11] proposed the possibility of the FCC phase in a certain pressure based on first-principles investigations. Moreover, Zhu et al. [12] proved that the existence of the interface layer and the FCC phase by using in situ heating based on the high-temperature instability of Ti-hydride. Hong et al. [13] observed the stress-induced FCC phase in pure titanium and considered that the stress-induced phase transformation was attributed to the gliding of Shockley partial dislocations, which provides a new plastic deformation martensite transformation mode. In general, most stress-induced HCP  $\rightarrow$  FCC phase transitions are caused by severe plastic deformation conditions, such as cryogenic channel-die compression, high energy shot peening, and cold rolling [14].

Recently, Zhao *et al.* [15] reported that the  $\alpha/\beta$  interface layer hindered dislocation motion and formed deformed twins, which significantly decreased the mean free path for dislocation slip to improve the strength of Ti-6Al-4V titanium alloy. Bai et al. [16] observed that the FCC phase has undergone various deformation modes such as shearing, bending, kinking, and their combinations in the rolling process, and considered that the kinking of the FCC band structure could lead to grain refinement and improve ductility. In sum, the interface layer and the FCC phase have a significant effect on the microstructure and properties of titanium and titanium alloys.

In addition, alloying elements always have a significant effect on the phase stability and microstructure control of alloy. Sahara et al. [17] reported that the hcp phase was more stable than the bcc phase when V, Cr, and Nb were added, whereas the bcc phase was stabilized when Fe, Co, and Mo are added. Lu et al. [18] found that some metastable  $\beta$  phases began to appear, when 3 or 5 wt% Mo was added to Ti-6Al-based alloys. Jiang et al. [19] found that the microhardness, mechanical strength, and plasticity of Ti-Zr alloy were increased concurrently as the Zr addition increased, observed that the interactions of twins caused the brittle fracture of Ti20Zr alloy, and proposed that the FCC phase impeded dislocation slip effectively, thereby improving the strength plasticity of Ti30Zr alloy. It can be concluded that optimizing the type and the content of alloying elements is a significant way to design high-strength various alloys to meet the strict requirements of modern industry.

Currently, the studies on the  $\alpha/\beta$  interface layer and the FCC phase of titanium alloys are mainly focused on pure titanium and Ti-6Al-4V titanium alloy. Moreover,

the investigation on the formation mechanism of the FCC phase is also mainly concentrated on plastic deformation. As a significant method to strengthen the properties of titanium alloys, element addition also should have a complex influence on the  $\alpha/\beta$  interface layer and the FCC phase. However, few scholars pay attention to the  $\alpha/\beta$ interface layer and the FCC phase of multi-element near α titanium alloys. Moreover, the influence mechanism of the alloying elements on the formation of the FCC phase in titanium alloys is still unclear.

Multi-element near α titanium alloys always have more complex alloving elements and more excellent welding performance and impact toughness than pure titanium and Ti-6Al-4V titanium alloys. Studying the interface layer and the FCC phase of the multi-element near  $\alpha$  titanium alloy is beneficial to control the microstructure and improve the comprehensive properties of near α titanium alloy. In addition, explaining the influence mechanism of elements on the FCC phase can be conducive to the design of titanium alloy with better properties by optimizing the composition of alloy elements. Therefore, it is necessary to study the interface layer and the FCC phase of the multi-element near  $\alpha$  titanium alloy.

In this article, near α Ti80 titanium alloy with a nominal composition of Ti-6Al-3Nb-2Zr-1Mo was selected as the study material, which is developed by adjusting the element type of Ti-6Al-4V alloy [20,21]. The structure of the  $\alpha/\beta$  interface layer of Ti80 alloys was studied by using TEM, and the orientation relationship of the  $\alpha$  phase, the β phase, and the FCC phase of the alloy are determined. In addition, a nanoscale strain analysis of the interface layer and the FCC phase of the titanium alloy was first studied by using the geometry phase analysis (GPA). Finally, the element distribution of the  $\alpha/\beta$  interface layer was observed by using scanning transmission electron microscopy (STEM), and the influence of alloying elements on the formation of the FCC phase was discussed. This study can provide a new idea for optimizing the microstructure and properties of titanium alloys.

# 2 Experimental procedure

The as-received material used in this investigation is forged Ti80 titanium alloy, which is prepared by vacuum arc melting and forging processes. The chemical composition of Ti80 alloy is presented in Table 1. The β-transus temperature of the alloy is 1,000°C  $\pm$  7°C [22]. The annealing treatment temperature was selected at 20°C above and below the β-transus temperature and at a lower temperature

Table 1: The chemical composition of Ti80 alloy (mass fraction, %)

Sample	Ti	Al	Nb	Zr	Мо	N	Н	0
Ti80	Bal.	6.50	3.18	2.04	1.17	0.0016	0.0060	0.113

of 900°C to obtain three typical structures of titanium alloys: equiaxed, bimodal, and lamellar structures. The cooling method was air cooling (AC). The specific heat treatment process is 900°C  $\times$  1 h/AC (equiaxed structure), 980°C  $\times$  1 h/AC (bimodal structure), and 1,020°C  $\times$  0.5 h/AC (lamellar structure).

The samples for metallographic observation were cut  $15~\text{mm} \times 15~\text{mm} \times 15~\text{mm}$  from forged and annealed Ti80 alloy by using electric discharge wire-cutting technology. The specimens were polished and etched with a Kroll's reagent (2%HF + 8%HNO<sub>3</sub> + 90%H<sub>2</sub>O). Subsequently, some square sheets with a thickness of 0.3 mm and a side length of 10 mm were cut from the sample for TEM observation. The discs with a diameter of 3 mm were punched out after being mechanically thinned to 80  $\mu$ m. The discs were further polished by twin-jet electropolishing technique. The electropolishing solution is composed of 5% perchloric, 35% butanol, and acid 60% methanol. The microstructure of Ti80 alloy was observed by using Zeiss axiovert A1 optical microscope (OM) and

JEM-2100 transmission electron microscope, and then, the element distribution was analyzed by JEM-200F scanning transmission electron microscopy.

### 3 Results

# 3.1 Microstructural characteristics of Ti80 alloy with different states

Figure 1 shows the metallographic images of Ti80 alloy with different states. Light-colored blocks, light-colored needles, and dark-colored strips represent the primary  $\alpha$  phase, secondary  $\alpha$  phase, and residual  $\beta$  phase, respectively. Figure 1(a) shows the metallographic microstructure of the initial forged state. It can be observed that the grains are elongated, indicating the microstructure still retains the characteristics of forging deformation. In addition, some regions surrounded by the primary  $\alpha$  phase have complex structures, which may include  $\beta$  phase,  $\alpha'$  phase, interfacial layer, and so on, which cannot be clearly observed under the metallurgical microscope, as marked by the white circle. Figure 1(b)–(d) shows the metallographic images of the alloy after  $900^{\circ}\text{C} \times 1\,\text{h/A}$ ,  $980^{\circ}\text{C} \times 1\,\text{h/AC}$ , and  $1,020^{\circ}\text{C} \times 1\,\text{h/AC}$ ,

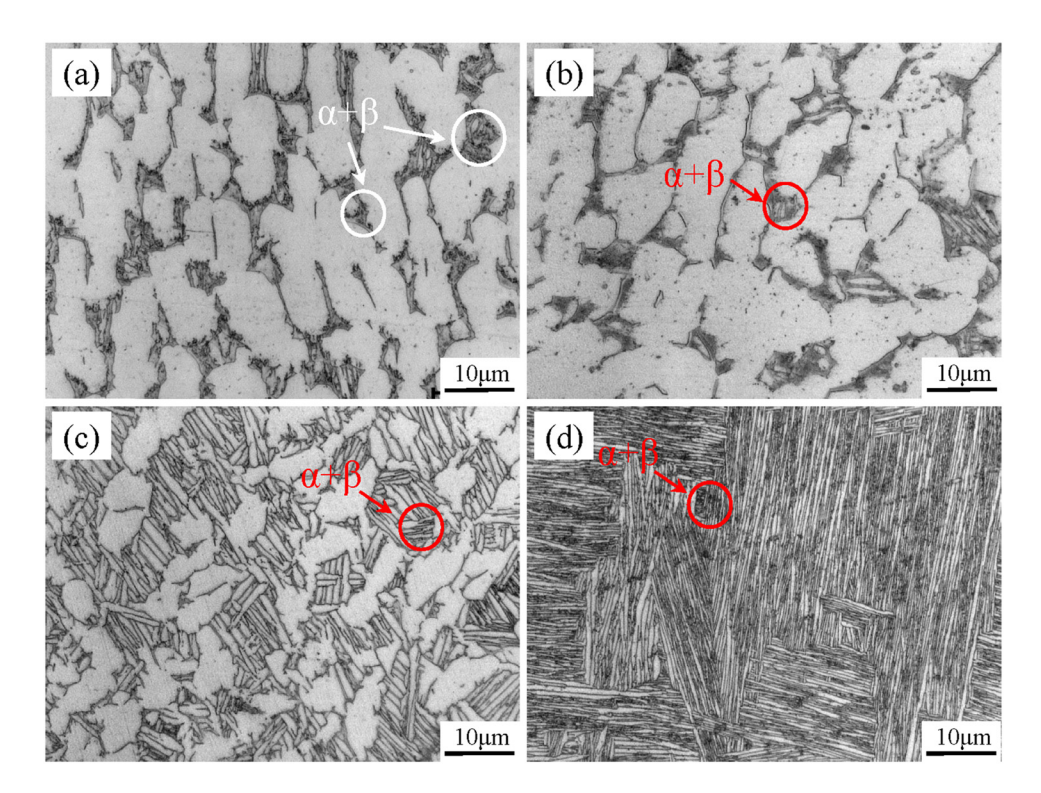


Figure 1: Metallographic images of Ti80 alloy: (a) as-forged, (b)  $900^{\circ}\text{C} \times 1 \text{ h/AC}$ , (c)  $980^{\circ}\text{C} \times 1 \text{ h/AC}$ , and (d)  $1,020^{\circ}\text{C} \times 0.5 \text{ h/AC}$ .

which present three typical microstructures of titanium alloys: equiaxed, bimodal, and lamellar state, respectively. Obviously, as the annealing temperature increases, the proportion and the thickness of the lamellar grains gradually increase and decrease, respectively, which should be attributed to the  $\alpha \to \beta$  phase transition of the alloy. In addition, there are also some complex  $\alpha + \beta$  phase regions that cannot be clearly observed in Ti80 alloys with equiaxed, bimodal, and lamellar structures, which may contain the  $\alpha/\beta$  interface layer, as shown by the red circle. In general, there may be an interface layer in the four Ti80 alloys, but it cannot be cleared from the metallographic images. Therefore, the TEM was used to observe the microstructure of Ti80 alloy with four different states.

Figure 2 shows the TEM micrographs of Ti80 alloy with different states in different microstructure regions. It can be observed from Figure 2(a) that the interior of the  $\alpha$  phase of forged Ti80 alloy comprised many dislocations. In addition, there is a short strip of  $\beta$  grain between two  $\alpha$  grains, and a very narrow interface layer with a thickness of less than 200 nm (represented by J in figure) was observed between  $\alpha$  phase and  $\beta$  phase. Figure 2(b) shows TEM micrographs of the trigeminal grain boundary region between  $\alpha$  grains of equiaxed Ti80 alloy. It can be seen that the needle-like  $\alpha'$  phase is evenly distributed in the  $\beta$  phase, and there are interface layers with a thickness of about 200 nm between the trifurcated region and

 $\alpha$  grains. Figure 2(c) shows the TEM structure at the boundary between the  $\alpha$  phase and the  $(\alpha + \beta)$  region in Ti80 alloy with a bimodal structure. It also can be seen that the interface layer with a thickness of about 150 nm between  $\alpha$  and  $\beta$  grains, which manifested as high-density dislocations. Figure 2(d) shows the lamellae  $\alpha + \beta$ region of Ti80 alloy with a lamellar structure. An obvious interface layer with a thickness of about 80 nm between the lamellar  $\alpha$  grain and the  $\beta$  grain can be found, which have a crystal structure different from matrix  $\alpha$  and  $\beta$ phases. In addition, in various annealed Ti80 alloys, the dislocations in  $\alpha$  phase almost disappear, but the interface layer and the β phase remain high-density dislocations. In general, it can be summarized that there are always interface layers between  $\alpha$  and  $\beta$  in different microstructure regions of the alloy with different states. Moreover, the interface layer shows different thicknesses in different microstructure regions and is mainly manifested as high-density dislocation stripes.

# 3.2 Structural characterization of $\alpha/\beta$ interface layer

Figure 3 shows the TEM micrographs of the forged Ti80 alloy and the selected area electron diffraction (SAED) pattern. Figure 3(a) also shows that there is an interface

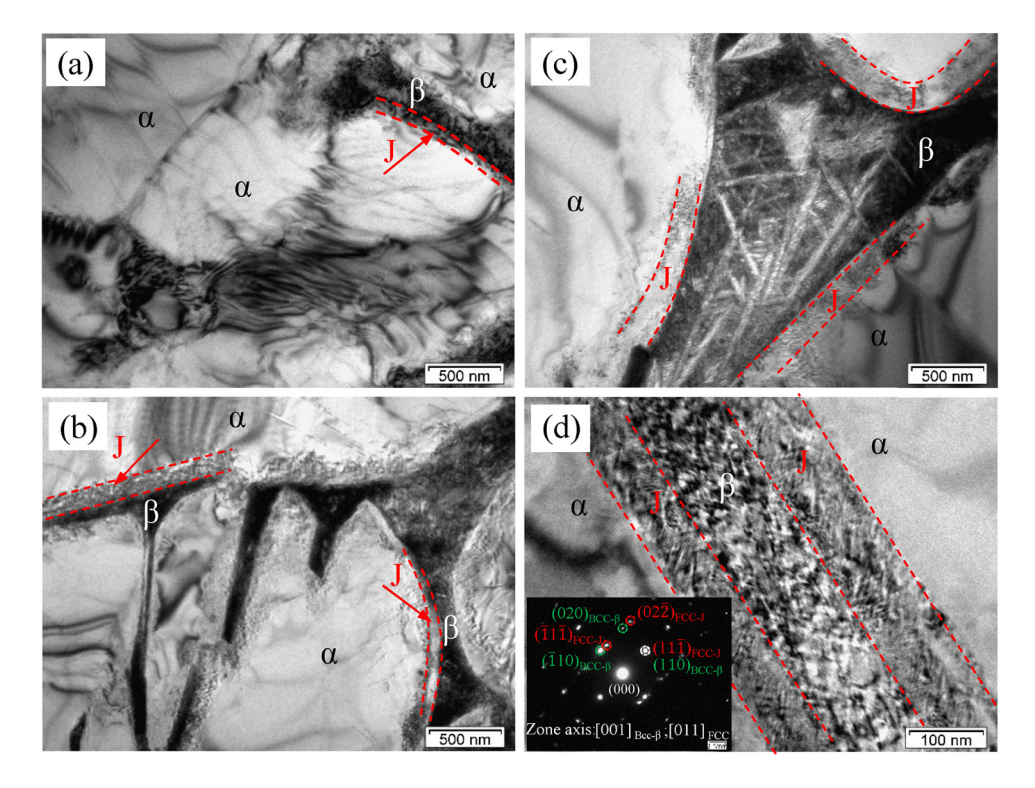


Figure 2: TEM micrographs of Ti80 alloy: (a) forged state ( $\alpha$  and  $\alpha$  grain region), (b) equiaxed state (trigeminal grain boundary region between equiaxed  $\alpha$  grains), (c) bimodal state ( $\alpha$  and  $\alpha + \beta$  region), and (d) lamellar state (lamellar  $\alpha + \beta$  region).

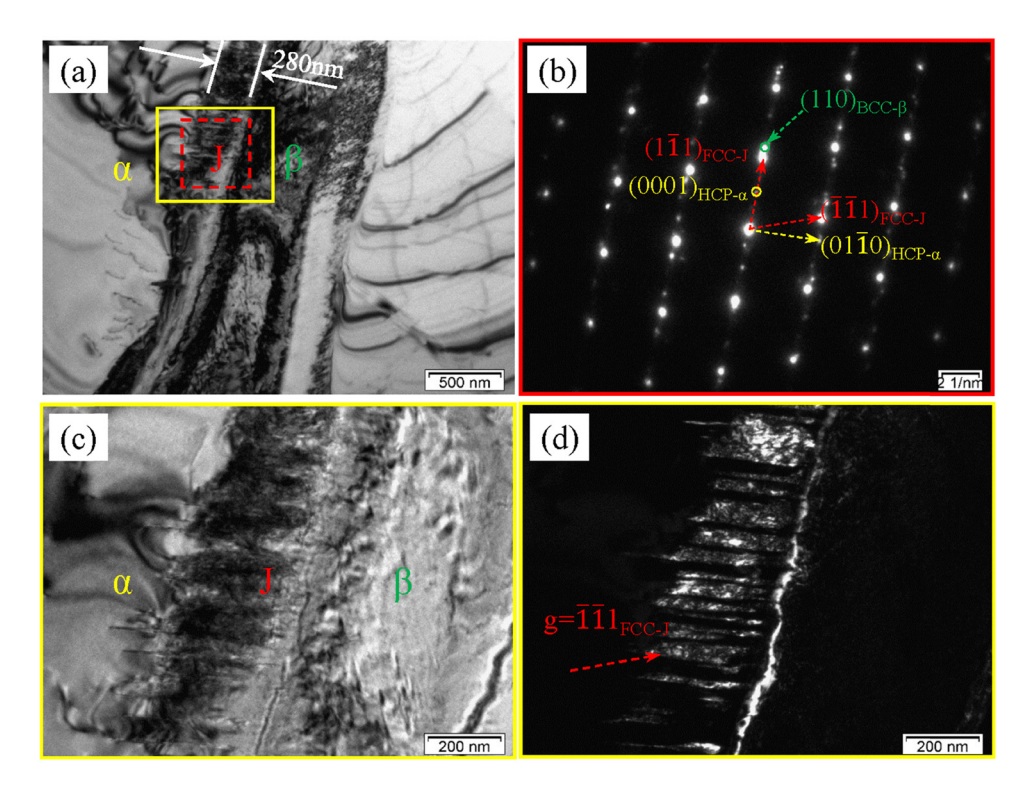


Figure 3: TEM micrographs of forged Ti80 alloy: (a) bright-field image, (b) selected area electron diffraction (SAED) in the red rectangle of (c), (c) partial magnification images of yellow rectangle of (c), and (d) the dark field image of (c).

layer with a thickness of about 280 nm between the a phase with some dislocation lines and the  $\beta$  phase with high-density dislocations. Figure 3(b) shows the SAED pattern in the red rectangle region. After calibration, it can be known that this region is mainly composed of body-centered cubic (BCC) structure β phase, hexagonal close-packed (HCP) structure α phase, and face-centered cubic structure FCC phase. At the same time, it can be known that the orientation relationship of the  $\beta$  phase, the  $\alpha$  phase, and the FCC phase is  $(110)_{B}/(0001)_{\alpha}/$  $(1\bar{1}1)_{FCC}$  and  $[\bar{1}11]_{B}//[2\bar{1}\bar{1}0]_{\alpha}//[011]_{FCC}$ . Figure 3(c) shows the enlarged image of the yellow rectangle region in Figure 3(a). It can be seen that the FCC phase has high dislocation density. Previous studies have shown that the  $\alpha/\beta$  phase interface layer has the function of hindering the movement of dislocations [15], which would lead to the accumulation of considerable dislocations at the  $\alpha/\beta$ interface layer. Figure 3(d) shows the dark field image of Figure 3(a). It can be seen that these FCC phases mainly show lamellar, which are perpendicular to the β phase, and there may be a twinning relationship between these lamellar FCC phases. In addition, it can also be seen that the boundary between the lamellar FCC phase and the  $\alpha$ phase is zigzag, and the junction with the  $\beta$  phase is relatively straight. To sum up, the  $\alpha/\beta$  interface layer is

mainly composed of lamellar FCC phases, which may have a twin relationship.

To further study the lamellar FCC phase of the interface layer, HRTEM observation was carried out on the J region in Figure 3(a), as shown in Figure 4. Figure 4(a)-(c) shows the HRTEM image, the partial fast Fourier transformation (FFT) and the local inverse Fourier transform (IFFT) image. It can be confirmed that the lamellar FCC phases does have twin relationship, and the zone axis and the twin plane are [011] and (111), respectively. It can be seen that the twin boundary exhibits ladder, and some interfaces have a coherent relationship. Figure 4(c) and (d) shows lattice fringes of the twin FCC phase region obtained by filtering, and it can be found that the twin lamellar FCC phases have high dislocation density, which indicates that there may be considerable phase transition stress during the formation process of the FCC phase. The value of measured ( $1\overline{1}1$ ) crystal plane spacing *d* is 0.2494 nm, and subsequently, the lattice parameter a of the FCC phase calculated is 0.4319 nm ( $a = d\sqrt{h^2 + k^2 + l^2}$ ). The formation of ladder FCC twins in the forged Ti80 alloy indicates that there may be a new deformation mechanism in the forging

Figure 5 shows the TEM micrographs of the disordered interface layer region in the forged Ti80 alloy.

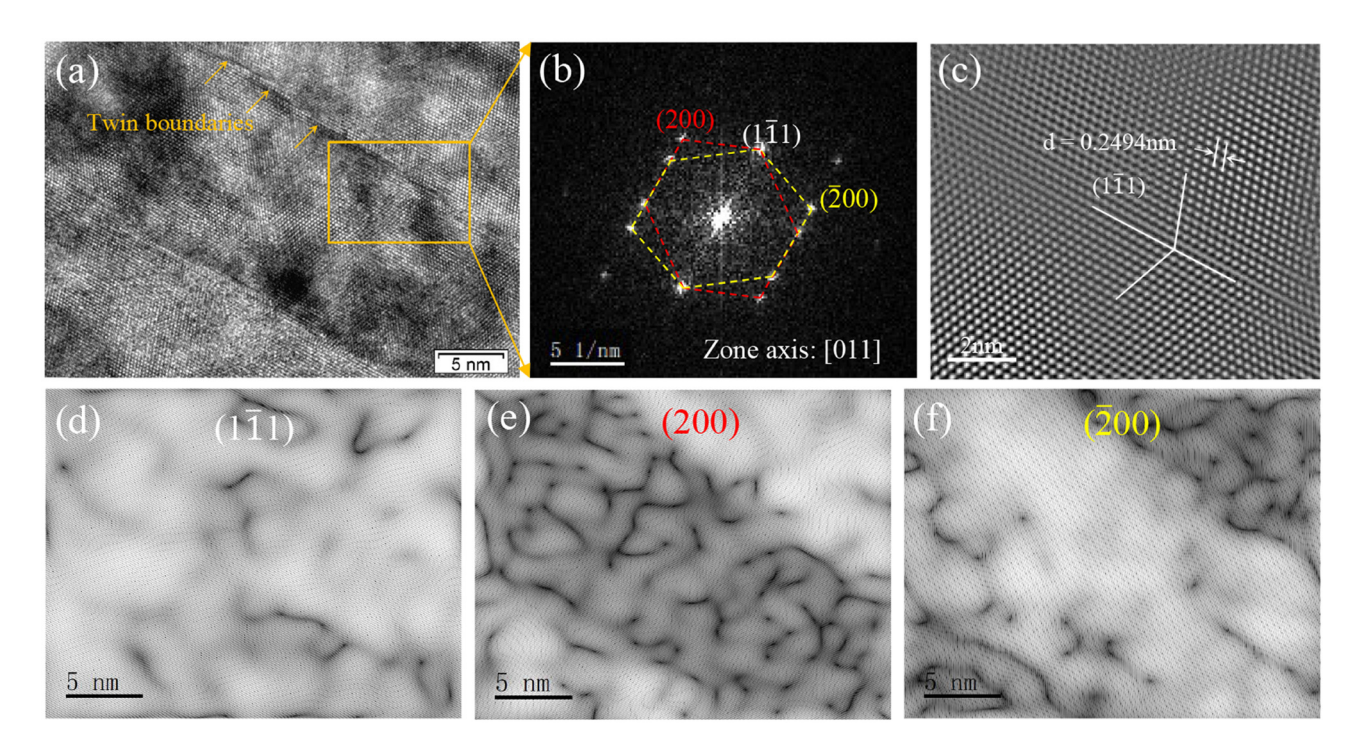


Figure 4: The partial HRTEM images of the J region of Figure 3(a) of: (a) HRTEM image of FCC phase, (b) FFT of orange rectangle in  $\mathbb{O}$ , (c) partial IFFT of (a), (d-f)  $(1\overline{1}1)_{FCC}$ ,  $(200)_{FCC}$ , and  $(\overline{2}00)_{FCC}$  lattice fringes of (a) obtained by filtering.

Figure 5(a) and (b) show a bright-field image and the partial SAED pattern. It can be observed from that the interface layer with a thickness of about 200 nm between

the left of the stripe  $\beta$  phase and  $\alpha$  phase, which is mainly composed of lamellar FCC phases. In addition, there is a 500 nm thick interface layer between the right of the

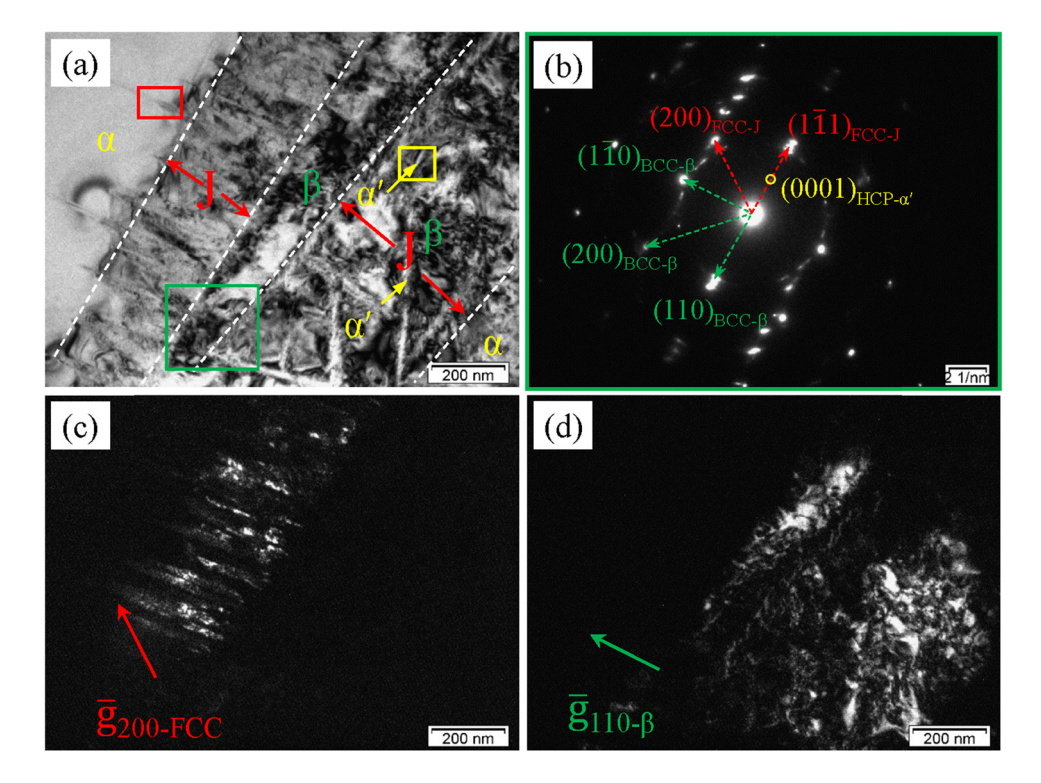


Figure 5: TEM micrographs of the disordered region in the forged Ti80 alloy: (a) bright-field image, (b) the SAED pattern in blue rectangle of (a), and (c) and (d) dark-field image of (a).

stripe  $\beta$  phase and  $\alpha$  phase has a different morphology and structure. The right interface layer is mainly composed of needle-like  $\alpha'$  phase and  $\beta$  phase with highdensity dislocation. At the same time, the partial SAED pattern confirms that the orientation relationships among β phase, FCC phase, and α' phase are  $(110)_{\rm B}//(1\bar{1}1)_{\rm FCC}//$  $(0001)_{\alpha'}$  and  $[001]_{\beta}//[011]_{FCC}//[2\bar{1}\bar{1}0]_{\alpha'}$ , which is consistent with the aforementioned calibration results. Figure 4(c) is the dark-field image of (a). It can be observed the lamellar FCC phases in the interface layer are perpendicular to strip the β phase, which shows a structure similar to Figure 3(d). Figure 4(d) shows the  $g_{110-\beta}$  dark-field image. The bright region is the stripe  $\beta$  phase and the  $\beta$ phase of the right  $\beta + \alpha'$  mixed zone. It can be found that lots of dislocations accumulate in the β phase after forging deformation, which may cause the distortion of  $\beta$ phase crystal lattice and induce the formation of the  $\alpha'$ phase.

Figure 6(a) shows the HRTEM image and local lattice fringes of  $\beta$  and  $\alpha'$  phases. It can be seen that the lattice fringes of the  $\beta$  phase are relatively regular, while the lattice fringes of the needle-like  $\alpha'$  phase are arranged in a disorderly manner, indicating  $\alpha'$  phase has a high dislocation density. Generally speaking, the lattice parameter a and c of  $\alpha'$  phase are 0.308 and 0.47 nm, slightly higher than the lattice parameter of  $\alpha$  phase (a = 0.2944 nm and c = 0.4678 nm), respectively. The generation of  $\alpha'$  phase is mainly related to the  $\beta \rightarrow \alpha$  phase transition during the cooling process [23]. Figure 6(b) shows the HRTEM image, FFT pattern, and local lattice fringes of the FCC phase and the  $\alpha$  phase. It can be seen that the FCC phase located at the  $\alpha/\beta$  interface layer gradually grows into  $\alpha$  phase matrix along the  $[0\bar{1}10]_{FCC}$ . In addition, obviously, there are lots

of dislocations at the interface between the FCC phase and the matrix  $\alpha$  phase in the interface layer. The growth of the FCC phase into the  $\alpha$  phase destroys the atomic arrangement of the matrix  $\alpha$  phase, which leads to a higher dislocation density at the junction of FCC and  $\alpha$  phases. The orientation relationship calibrated between the FCC phase and the  $\alpha$  phase are  $(1\bar{1}1)_{FCC}/(0001)\alpha$  and  $[011]_{FCC}/[2\bar{1}\bar{1}0]_{\alpha}$ , which are consistent with the aforementioned calibration results.

Elements have a significant influence on the formation of the phase in titanium alloy [24]. Therefore, it is necessary to observe the element distribution of the alloy and study its influence on the formation of the interface layer. Figure 7 shows the elemental analysis of the lamellar  $\alpha/\beta$  phases and the interface layer between the two phases. It can be found that Ti and Al elements are considerably concentrated in the  $\alpha$  phase, and the distribution of Ti and Al elements in the  $\alpha$  phase, the  $\beta$  phase, and the interface layer has a concentration gradient. Moreover, the gradient distribution of Al is more significant. The distribution of both Mo and Nb has a concentration in the  $\beta$  phase, especially the Mo element is more obvious. In addition, there is no obvious difference in the distribution of Zr elements in the  $\alpha$  phase, the  $\beta$  phase, and the interface layer.

### 4 Discussion

#### 4.1 Nanoscale strain field analysis

A nanoscale strain field will be formed in the FCC +  $\alpha$  and  $\alpha'$  +  $\beta$  regions due to the difference in their lattice constants. The strain field has a significant effect on

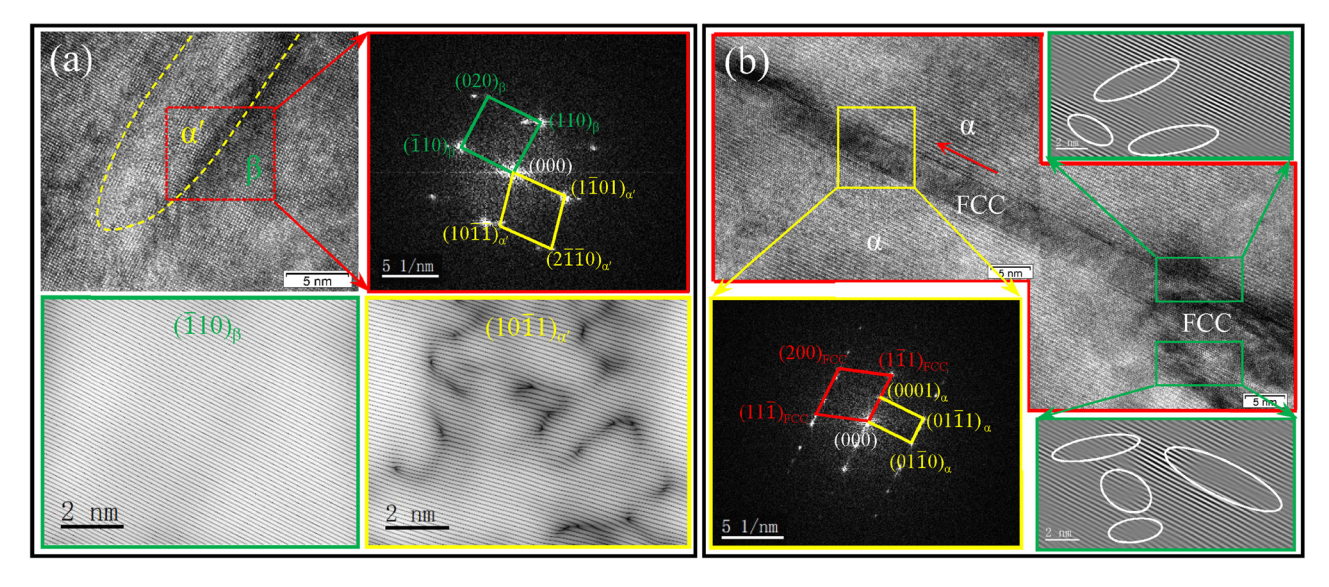


Figure 6: TEM micrographs of the yellow and red rectangle region in Figure 5(a): (a) the HRTEM image FFT pattern,  $(0\bar{1}10)_{\alpha'}$  and  $(\bar{1}10)_{\beta}$  lattice fringes of  $(\alpha' + \beta)$  region, (b) the HRTEM image, FFT pattern, and  $(1\bar{1}1)_{FCC}$  lattice fringes obtained by filtering of (FCC +  $\alpha$ ) region.

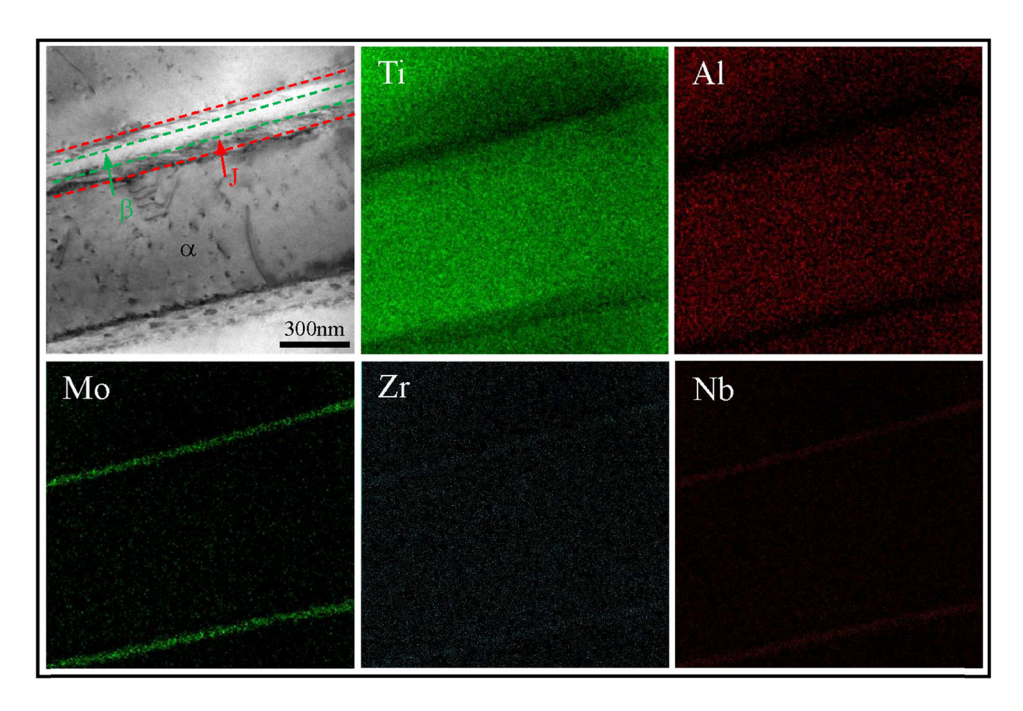
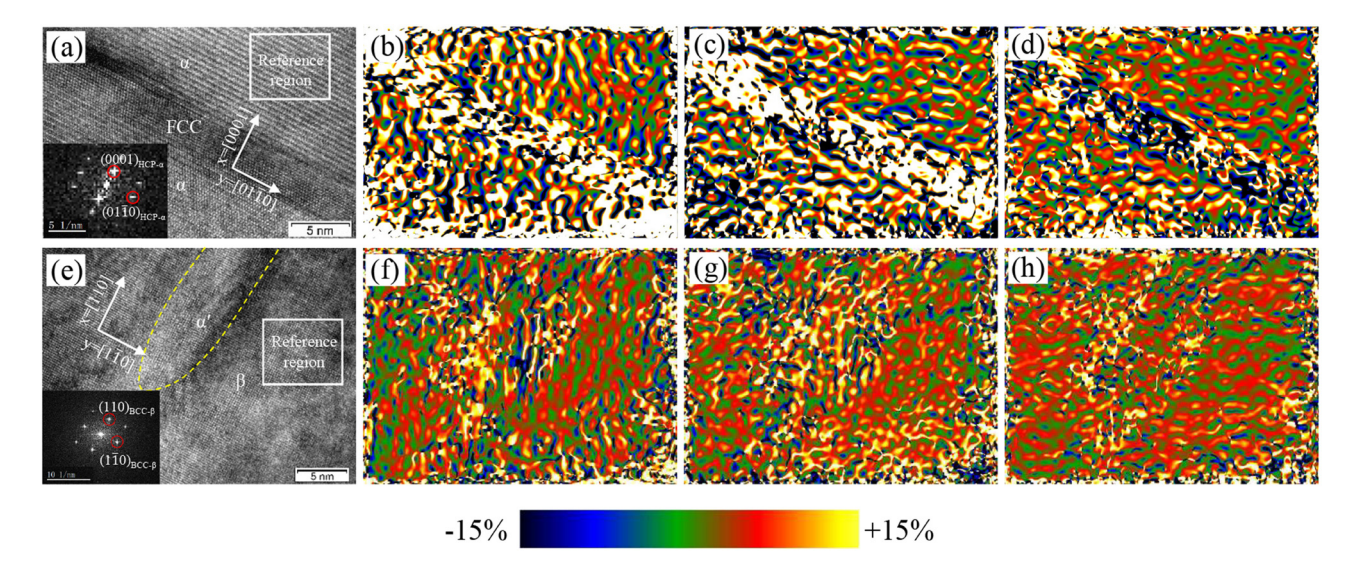


Figure 7: STEM element distribution diagram of forged Ti80 alloy.

hindering the movement of dislocations and the formation and the growth of precipitates [25]. In this study, the geometric phase analysis (GPA) was introduced to analyze the strain field of the  $\alpha/\beta$  interface layer. GPA is an image-processing technique for measuring atomic displacements recorded in HRTEM images, and the displacement as small as 0.003 nm can be detected [26]. The principle of GPA is that the HRTEM images formed on a certain zone axis can be regarded as a series of interference

fringes corresponding to the atomic plane, subsequently, the relevant strain information can be obtained by analyzing these interference fringes. Figure 8(a) and (e) shows HRTEM images of FCC +  $\alpha$  and  $\alpha'$  +  $\beta$  regions, respectively. Figure 8(b)–(d) shows the strain fields of  $\varepsilon_{xx}$ ,  $\varepsilon_{xy}$ , and  $\varepsilon_{yy}$  corresponding to Figure 8(a), and Figure 8(f)–(h) show the strain fields of  $\varepsilon_{xx}$ ,  $\varepsilon_{xy}$ , and  $\varepsilon_{yy}$  corresponding to Figure 8(e). The positive value in Figure 8 represents tensile strain and vice versa represents compressive strain. It can be



**Figure 8:** The strain fields of FCC +  $\alpha$  and  $\alpha'$  +  $\beta$  regions obtained by the geometric phase analysis: (a) and (e) HRTEM images corresponding to FCC +  $\alpha$  and  $\alpha'$  +  $\beta$ , (b-d) the strain component  $\varepsilon_{xx}$ ,  $\varepsilon_{xy}$ , and  $\varepsilon_{yy}$  of (a), and (f)-(h) the strain component  $\varepsilon_{xx}$ ,  $\varepsilon_{xy}$ , and  $\varepsilon_{yy}$  of (e).

observed that the overall strain gradient of the FCC +  $\alpha$ region is larger than the  $\alpha' + \beta$  region. Furthermore, it can be seen from Figure 8(a)-(d) that the internal of the FCC phase shows the considerable strain compared with the surrounding α phase matrix, indicating that the FCC phase undergoes severe lattice distortion during the formation process. In addition, the strain field components  $\varepsilon_{xx}$  and  $\varepsilon_{xy}$  of the FCC phase are mainly tensile strains, while the strain component  $\varepsilon_{vv}$  is mainly compressive strain. It can be seen from Figure 8(e)–(f) that the internal strain of the  $\alpha'$  phase is larger than the  $\beta$  phase, the latter exhibits lower strain. In addition, the strain field components  $\varepsilon_{xx}$  and  $\varepsilon_{xy}$ of  $\alpha'$  phase are more significant than  $\varepsilon_{yy}$ , and the high strain region of the component  $\varepsilon_{vv}$  is mainly concentrated at the junction of  $\alpha'$  phase and  $\beta$  phase. In general, FCC +  $\alpha$ region show more significant strain gradient than  $\alpha' + \beta$ region, and  $\varepsilon_{FCC} > \varepsilon_{\alpha}$ ,  $\varepsilon_{\alpha'} > \varepsilon_{\beta}$ .

## 4.2 Formation mechanism of FCC phase of the $\alpha/\beta$ interface layer

After the aforementioned analysis of the characterization and orientation relationship of the interface layer, the schematic diagram of microstructure morphology and orientation relationship of the interface layer was constructed, as shown in Figure 9. Currently, deformationinduced FCC phase formation has been clearly studied and mainly attributed to the sliding of Shockley partial

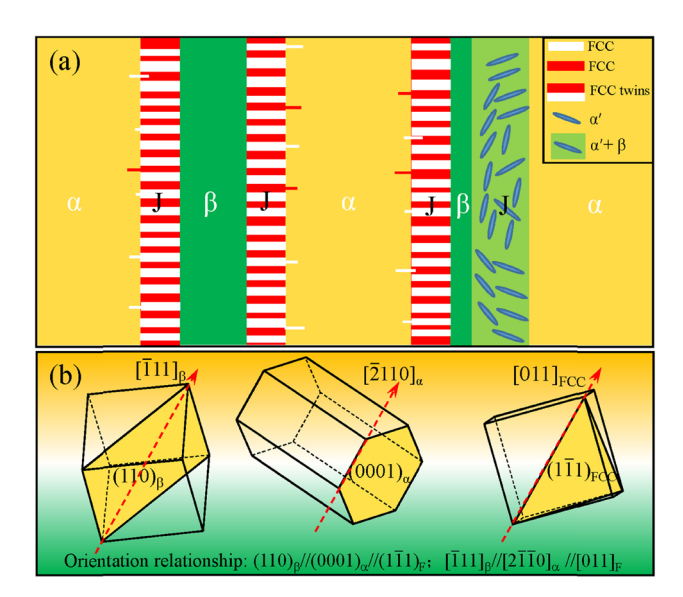


Figure 9: Schematic diagram of interface layer and FCC phase: (a) microstructure morphology and (b) orientation relationship.

dislocations [12]. However, in this study, it can be seen that not only the FCC phase appears in the forged Ti80 alloy but also in the annealed state, which proves that there should be other reasons leading and facilitating the FCC phase besides the deformation-induced phase transformation. Ti80 titanium alloy has more complex element types than pure titanium and Ti-6Al-4V alloy. To improve the mechanical properties of the alloy, Zr was added to Ti80 titanium alloy as a strengthening element. As generally known, the atomic radius of Zr is 0.162 nm larger than titanium (0.147 nm) [27], which will cause lattice distortion, and leads to a nanoscale strain field around the different atoms and interfaces/interphases. The interaction between the two strain fields may provide a driving force for the formation of the FCC phase. In addition, since Zr has lower the basal plane stacking fault energy than Ti [28], the addition of Zr may decrease the basal stacking fault energy of the α phase, thereby promoting the formation of the FCC phase. On the other hand, previous studies [29] have proposed that the interface FCC phase can be regarded as the intermediate phase in the  $\beta \rightarrow \alpha$  transformation process during the cooling of titanium alloy. The  $\beta$ phase-stabilizing elements such as Mo and V will generate a concentration gradient distribution due to its asymmetric diffusion during cooling [30], which will provide a chemical driving force for the FCC phase. However, in this study, it can be found from Figure 7 that there is no obvious concentration gradient of β phase stable elements (Mo and Nb), indicating that the FCC phase in this study should not be related to the concentration distribution of Mo and Nb. Moreover, it is interesting that there is an obvious concentration gradient of α phase-stabilizing element Al around the interface layer, which will cause the existence of stress around the  $\alpha/\beta$  phase interface layer. The  $\alpha/\beta$  interface layer will arise complex shear deformation under the effect of the chemical driving force, which leads to the formation of FCC twins. So, the concentration gradient of the Al element around the interface layer provides a chemical driving force for the formation of the FCC phase.

### 5 Conclusion

(1) The  $\alpha/\beta$  interface layer was found in the forged, equiaxed, bimodal, and lamellar Ti80 alloy. The interface layer mainly exhibits high-density dislocations and is mainly composed of the lamellar FCC phase region and  $\beta + \alpha'$  region. The thickness of the FCC phase region of the interface layer is within the range

- of 300 nm, and the  $\beta + \alpha'$  region shows a larger thickness, approximately 500 nm.
- (2) There is a twin relationship between the FCC phases in the interface layer, and the twin plane is  $(1\overline{1}1)$ . In addition, the FCC phase can grow into the matrix  $\alpha$ phase. The positional relationship of the  $\beta$  phase, the  $\alpha$ phase, and the FCC phase is  $(110)_{\beta}//(0001)_{\alpha}//(1\overline{1}1)_{FCC}$ ;  $[\bar{1}11]_{\rm g}//[2\bar{1}\bar{1}0]_{\rm g}//[011]_{\rm ECC}$ . FCC +  $\alpha$  region shows more significant strain gradient than  $\alpha' + \beta$  region, and  $\varepsilon_{FCC} > \varepsilon_{\alpha}, \ \varepsilon_{\alpha'} > \varepsilon_{\beta}.$
- (3) The addition of elements has a significant effect on the formation of the FCC phase. The addition of Zr promotes the formation of the FCC phase by inducing lattice distortion and reducing the stacking fault energy of the α phase. In addition, the Al element forms a significant concentration gradient around the FCC phase of the  $\alpha/\beta$  interface layer during the cooling process, which provides a driving force for the formation of the FCC phase.

Funding information: Henan Province "Innovative Science and Technology Team" Program (182101510003).

**Author contributions:** All authors have accepted responsibility for the entire content of this manuscript and approved its submission.

Conflict of interest: The authors state no conflict of interest.

### References

- Zhang ZX, Fan JK, Tang B, Kou HC, Wang J, Wang X, et al. Microstructural evolution and FCC twinning behavior during hot deformation of high temperature titanium alloy Ti65. J Mater Sci Technol. 2020;49:56-69.
- [2] Grishkov V, Kopylov V, Lotkov A, Latushkina S, Baturin A, Girsova N, et al. Effect of warm equal channel angular pressing on the structure and mechanical properties of Ti<sub>0.1</sub>6Pd<sub>0.14</sub>Fe (wt%) alloy. Rev Adv Mater Sci. 2019;58:22-31.
- Jonas JJ, Aranas JC, Fall A, Jahazi M. Transformation softening in three titanium alloys. Mater Des. 2017;113:305-10.
- Lin NM, Xie RZ, Zou JJ, Qin JF, Wang YT, Yuan S. Surface damage mitigation of titanium and its alloys via thermal oxidation: a brief review. Rev Adv Mater Sci. 2019;58:132-46.
- Wang Q, Ren JQ, Wu YK, Jiang P, Li JQ, Sun ZJ, et al. Comparative study of crack growth behaviors of fully-lamellar and bi-lamellar Ti-6Al-3Nb-2Zr-1Mo alloy. J Alloys Compd. 2019;789:249-55.

- Chen W, Lv YP, Zhang XY, Chen C, Lin YC, Zhou KC. Comparing the evolution and deformation mechanisms of lamellar and equiaxed microstructures in near β-Ti alloys during hot deformation. Mater Sci Eng A. 2019;758:71-8.
- Zheng X, Gong MY, Xiong T, Ge HL, Yang LX, Zhou YT, et al. Deformation induced FCC lamellae and their interaction in commercial pure Ti. Scr Mater. 2019;162:326-30.
- Liu YG, Li MO, Liu HI, Deformation induced face-centered cubic titanium and its twinning behavior in Ti-6Al-4V. Scr Mater. 2016;119:5-8.
- Banerjee D, Williams JC. The effect of foil preparation technique on interface phase formation in Ti alloys. Scr Mater. 1983;17(9):1125-8.
- [10] Banerjee D, Shelton CG, Ralph B, Williams JC. A resolution of the interface phase problem in titanium alloys. Acta Metall. 1988;36(1):125-41.
- [11] Aguayo A, Murrieta G, Coss de R. Elastic stability and electronic structure of fcc Ti, Zr, and Hf: a first-principles study. Phys Rev B. 2002;65:092106.
- [12] Zhu W, Kou WJ, Tan CS, Zhang BY, Chen W, Sun QY, et al. Face centered cubic substructure and improved tensile property in a novel β titanium alloy Ti-5Al-4Zr-10Mo-3Cr. Mater Sci Eng A. 2020:771:138611.
- [13] Hong DH, Lee TW, Lim SH, Kim WY, Hwang SK. Stress-induced hexagonal close-packed to face-centered cubic phase transformation in commercial-purity titanium under cryogenic plane-strain compression. Scr Mater. 2013;69(5):405-8.
- [14] Kou W, Sun Q, Xiao L, Sun J. Plastic deformation-induced HCPto-FCC phase transformation in submicron-scale pure titanium pillars. J Mater Sci. 2020;55(5):2193-201.
- [15] Zhao Z, Chen J, Guo S, Tan H, Lin X, Huang W. Influence of  $\alpha/\beta$ interface phase on the tensile properties of laser cladding deposited Ti-6Al-4V titanium alloy. J Mater Sci Technol. 2017;33(7):675-81.
- [16] Bai FM, Yin LB, Zhao W, Zhou HW, Song M, Liu YC, et al. Deformational behavior of face-centered cubic (FCC) phase in high-pure titanium. Mater Sci Eng A. 2021;800:140287.
- [17] Sahara R, Emura S, Tsuchiya K. Theoretical investigation of effect of alloying elements on phase stability in body-centered cubic Ti-X alloys (X = V, Cr, Fe, Co, Nb, and Mo). J Alloys Compd. 2015;634:193-9.
- [18] Lu JW, Ge P, Zhao YQ, Niu HZ. Structure and mechanical properties of Ti-6Al based alloys with Mo addition. Mater Sci Eng A. 2013;584:41-6.
- [19] Jiang J, Zhao YW, Wang XX. Effects of Zr addition on the deformation behavior, microstructure and mechanical properties of dental Ti alloys. Mater Sci Eng A. 2020;794:139808.
- [20] Guo K, Meng K, Miao D, Wang Q, Zhang C, Wang T. Effect of annealing on microstructure and tensile properties of skew hot rolled Ti-6Al-3Nb-2Zr-1Mo alloy tube. Mater Sci Eng A. 2019:766:138346.
- [21] Zhou DD, Zeng WD, Xu JW, Chen W, Wang SM. Characterization of hot workability for a near alpha titanium alloy by integrating processing maps and constitutive relationship. Adv Eng Mater. 2019;21(7):1801232.
- [22] Su BX, Luo LS, Wang BB, Su YQ, Wang L, Ritchie RO, et al. Annealed microstructure dependent corrosion behavior of Ti-6Al-3Nb-2Zr-1Mo alloy. J Mater Sci Technol. 2021;62:234-48.

- [23] Guo Q, Wang Q, Han XL, Lu XK, Sun DL, Wu GH. Precipitation behavior of  $\alpha$  phase and mechanical properties in severely plastic deformed Ti-15-3 alloy. Rare Met Mater Eng. 2011;40(3):377-83.
- [24] Xu YQ, Fu Y, Li J, Xiao WL, Zhao XQ, Ma CL. Effects of tungsten addition on the microstructural stability and properties of Ti-6.5Al-2Sn-4Hf-2Nb-based high temperature titanium alloys. J Mater Sci Technol. 2021;93:147-56.
- [25] Chen YF, Yang B, Zhou YT, Wu Y, Zhu HH. Evaluation of pitting corrosion in duplex stainless steel Fe20Cr9Ni for nuclear power application. Acta Mater. 2020;197:172-83.
- [26] Chung J, Rabenberg L. A geometric phase analysis method dedicated to nanomaterials orienting along high-index zone axis. Micron. 2018;113:20-3.

- [27] Ji PF, Li B, Liu SG, Zhang X, Chen BH, Zhang XY, et al. Controlling the corrosion behavior of Ti-Zr alloy by tuning the  $\alpha/\beta$  phase volume fraction and morphology of  $\beta$  phase. J Alloys Compd. 2020;825:154153.
- [28] Ji PF, Chen BH, Li B, Tang YH, Zhang GF, Zhang XY, et al. Influence of Nb addition on microstructural evolution and compression mechanical properties of Ti-Zr alloys. J Mater Sci Technol. 2021;69:7-14.
- [29] Katzarov I, Malinov S, Sha W. Finite element modeling of the morphology of  $\beta$  to  $\alpha$  phase transformation in Ti-6Al-4V alloy. Metall Trans A. 2002;33(4):1027-40.
- [30] Huang C, Dean TA, Loretto MH. Interface phase in  $\alpha_2$  and B2 boundaries in Ti-25Al-10Nb-3V-1Mo alloy. Mater Sci Technol. 1995;11(2):143-9.